Appendix items

Seipin regulates ER-lipid droplet contacts and cargo delivery

Veijo T. Salo, Ilya Belevich[†], Shiqian Li[†], Leena Karhinen, Helena Vihinen, Corinne Vigouroux, Jocelyne Magré, Christoph Thiele, Maarit Hölttä-Vuori, Eija Jokitalo and Elina Ikonen

[†] Equal contribution

Table of contents

Appendix Materials and Methods

Antibodies, dyes and reagents. Rabbit anti-calreticulin (Thermo Scientific, PA3-900, IF 1:200), mouse anti-ACSL3 (Abnova, B01P, IF 1:200, immuno-EM 1:20), mouse anti-GFP (Roche, 11814460001, immuno-EM 1:50), rabbit anti-GFP (Abcam, ab290, STORM 1:800, IF 1:5000, WB: 1:10 000), rabbit anti-DGAT2 (Kuerschner *et al*, 2008) (IF 1:50), Alexa568 goat anti-rabbit (Thermo Scientific, A11008, IF 1:200), mouse anti-tubulin (Sigma, T5168, WB 1:10 0000), Alexa568 goat anti-mouse (Thermo Scientific, A11011, IF 1:200), Alexa647 donkey anti-mouse (Thermo Scientific, A31571, IF 1:200), Alexa647 donkey anti-rabbit (Molecular Probes A31573, STORM and IF 1:200); HCS LipidTox red (Thermo Scientific, H34476, fixed cells 1:200, live cells 1:1000), HCS LipidTox green (Thermo Scientific, H34475, fixed cells 1:200, live cells 1:1000), HCS LipidTox deep red (Thermo Scientific, H34477, live cells 1:2500), LD540 (Spandl *et al*, 2009) (Princeton BioMolecular Research, 1mg/ml, fixed cells 1:10 000, live cells A431 1:5000 and firboblasts 1:8000), DAPI (Sigma, 10µg/ml final concentration), Prolong Live Anti-Fade (Thermo Fisher, live cells 1:100); Lipofectamine LTX and Plus Reagent (Invitrogen); Hiperfect (Qiagen); PEG 1500 (Roche, 50% w/v in 75 mM Hepes); Vectashield (Vector Labs, H-1000). Other reagents, including cell culture reagents, were from Gibco/Thermo Fisher, Lonza and Sigma-Aldrich. Alkyne lipids were synthesized as described previously (Thiele *et al*, 2012).

Plasmids and siRNAs. To construct pEGFP-C1-ADRP, ADRP (cDNA accession number BC005127) was amplified by PCR and inserted into pEGFP-C1 (Clontech) via XhoI restriction site. For generation of pEFIRES-P-EGFP-ADRP, EGFP-ADRP coding sequence was cut from pEGFP-C1-ADRP and inserted into pEFIRES-P (Hobbs *et al*, 1998) (a gift from Dr. Olli Ritvos, Univ. of Helsinki) via NheI/EcoRI restriction sites. ACSL3 coding sequence (cDNA accession number NM_203372.1) was amplified by PCR from A431 cDNA. To construct pEFIRES-P-ACSL3-

mCherry, the fragment was cut with EcoRI and SalI, together with mCherry coding sequence from pmCherry-N1 (Clontech) cut with SalI and NotI, inserted into pEFIRES-P through EcoRI and NotI sites. For WT-seipin-mEGFP, WT-seipin(long)-mEGFP (used only in Appendix Fig S4B) and A212P-Seipin-mEGFP, WT-seipin (cDNA accession number BC012140), WT-seipin(long) (NM_001122955.3) and A212P-seipin (G822C point mutation of BC012140), coding sequences were amplified by PCR, cut with EcoRI and BamHI, together with a mEGFP coding fragment on the backbone of pEGFP-N3 (Clontech) cut with NotI, blunted with T4 DNA polymerase and cut with BamHI, then inserted into pBABEpuro vector (Morgenstern & Land, 1990) via EcoRI and blunted SalI sites. To construct HSP47-APEX-RDEL, GFP in Hsp47-GFP-RDEL (Kano *et al*, 2005) was replaced by APEX (Martell *et al*, 2012) by using PCR and subcloning into BamHI-NotI sites, creating Hsp47-APEX-RDEL. To construct HPos-mCherry, oligonucleotides encoding the HPos sequence (Kassan *et al*, 2013), followed by a TGA stop codon and flanked with a 5' BspEI restriction site and 3'blunt end, were synthesized, annealed and inserted into pmCherry-C1 via BspEI and SmaI restriction sites. This construct was then cut with BamHI, blunted with T4DNA polymerase, and cut with NheI. Finally the fragment was inserted into pEFIRES-P via NheI and blunted EcoRI restriction sites. ER marker peptides used in this study were pEFIRES-BFP-KDEL and sfGFP-ER-3. To construct pEFIRES-BFP-KDEL, mTagBFP-KDEL-C1 (a gift from Gia Voeltz, Addgene plasmid #49150 (Friedman *et al*, 2011)) was cut with KpnI, blunted with T4 DNA polymerase then cut with NheI and ligated into pEFIRES-P via NheI and blunted XhoI sites. sfGFP-ER-3 was a gift from Michael Davidson (Addgene plasmid # 56482). P-wt-human-DGAT2 plasmid has been described (Kuerschner *et al*, 2008). SiRNA against human seipin has been described (Hölttä-Vuori *et al*, 2013). SiRNAs against human ACLS3 (Ambion) were GGAACUAACUGAACUAGCU (sense) and AGCUAGUUCAGUUAGUUCC (antisense). Control siRNAs against firefly luciferase2 (GL2) have been described (Elbashir *et al*, 2001).

Generation of stable cell lines. To generate seipin knockout (SKO) cells, CRISPR/Cas9 technology was used (Sander & Joung, 2014). pSpCas9n(BB)-2A-GFP (PX461) was a gift from Feng Zhang (Addgene plasmid # 48140)(Ran *et al*, 2013). To enable puromycin selection, the sgRNA expression unit from pSpCas9n(BB)-2A-GFP(PX461) was transferred to a plasmid with puromycin selection cassette. Furthermore, Cas9n-2A-GFP was transferred to pcDNA4/His-MaxC plasmid and placed under the control of CMV_IE promoter. For selection of Cas9 nickase targets, common exon sequences closest to the common start codon of BSCL2 (Gene ID:26580) were chosen and analyzed at http://crispr.mit.edu/ (Ran *et al*, 2013). Pairs of targets showing effective knockdown efficiency and used for this study are shown in **Appendix Fig S1**. Corresponding DNA oligos were synthesized, annealed and subcloned into the sgRNA expression vector through BbsI sites. All puromycin selections and maintenance were performed with a concentration of 1 µg/ml. For generation of SKO A431 cell lines, cells were co-transfected with Cas9 nickase and two matching pairs of the sgRNA expressing plasmids and placed under puromycin selection for 48 h 24 h after transfection. Cells were cultured for additional 4 d with normal medium without puromycin and single clones were isolated on 96-well plates with limiting dilution. Finally, SKO single clones were identified by PCR-PAGE (Zhu *et al*, 2014) and LD phenotype. Clones used in the study were further verified by Sanger sequencing. For the majority of experiments, A431 WT and SKO (S2AB-15, **Appendix Fig S1**) were used. For SB-EM experiments, WT cells were first transfected with HSP47-APEX-RDEL and a single clone was selected. These cells were then subjected to CRISPR/Cas9 mediated seipin knockout as described, yielding WT (S2A2) and SKO (S2AB-21) cell lines (**Appendix Fig S1**) with stable expression of HSP47-APEX-RDEL. These cells were then transfected with pEFIRES-P-ACSL3-mCherry and a semistable pool, grown in medium containing puromycin, was used for light microscopy experiments. For ET, WT A431 or SKO (S3AB-2, **Appendix Fig S1)** cells were used. For generation of SKO + WT- and A212P-seipin-GFP cells, SKO (S3AB-2, **Appendix Fig S1**) were infected with empty retrovirus or retrovirus expressing WT or A212P-seipin-mEGFP according to

(Morgenstern & Land, 1990). Single clones were isolated using puromycin selection. Please note that SKO + WT-seipin-GFP(long) cells were used in this study only as an additional marker in Western blot in **Appendix Fig S4B**. For generation of ADRP-GFP and HPos-mCherry expressing cells, WT or SKO (S2AB-15, **Appendix Fig S1**) cells were transfected with pEFIRES-P-ADRP-mEGFP or pEIRES-P-HPos-mCherry and semistable pool was used to address protein localization to LDs. For FRAP experiments of HPos-mCherry, single clones of WT and SKO cells with similar levels of fluorescence were isolated.

Quantitative PCR. Total RNA was were isolated with Nucleospin® RNA kit (Macherey-Nagel) and reverse transcribed with ProtoScript® II First Strand cDNA Synthesis Kit (NEB). Real-time PCR was performed with Lightcycler 480 SYBR Green master mix (Roche Diagnostics) on LightCycler 480 Instrument II (Roche) with primers (0.5µM each, final concentration) at 62˚C annealing temperature. Analysis was performed by the ΔΔCT Method. Primer sequences are available upon request.

Western blotting. Cells were lysed in buffer containing 1.0% Igepal CA-630, 1.0 % sodium deoxycholate, and 0.1% sodium dodecyl sulfate with protease inhibitors. Equal amounts of protein were loaded onto SDS-PAGE and transferred to Hybond-C Extra Nitrocellulose membrane. Blotting was performed with Odyssey blocking buffer with IRDye 800CW donkey anti-rabbit and and IRDye 680LT donkey anti-mouse secondary antibodies (from LI-COR) according to the manufacturer's instructions. Images were acquired by scanning the membrane with Odyssey CLx near-infrared fluorescence imaging system.

Immunofluorescence. Cells grown on thickness 1.5 borosilicate glass coverslips were fixed with 4% paraformaldehyde in 250 mM HEPES, 100 µM CaCl, 100 µM MgCl, pH 7.4 for 20 min at RT, quenched with 50 mM NH_4Cl for 10 min at RT and if antibody stained, permeabilized with 0.1%

Triton X-100 for 4 min (anti-calreticulin) or 0.1% saponin for 10 min at RT (anti-ACLS3, anti-GFP, anti-DGAT2). For blocking (1 h RT) and primary and secondary antibody dilutions 10% FBS (anti-calreticulin, anti-DGAT2, anti-GFP for IF), 0.2% fatty-acid free BSA (anti-ACSL3) or 1% fatty-acid free BSA (anti-GFP for STORM) was used. Primary antibodies were incubated for 1 h at +37°C (anti-calreticulin) or RT (anti-ACSL3, anti-GFP, anti-DGAT2). Where indicated, LDs were stained with LD540, LipidTox Red or LipidTox Green and nuclei with DAPI, all diluted in PBS for 30 min at RT. Coverslips were mounted with Mowiol-Dabco. LD imaging was done within 24 h to minimize post-fixation artefacts. For 3D-SIM microscopy cells were mounted with Vectashield and sealed with nail polish.

Confocal microscopy. Cells were imaged using a Leica TCS CARS SP8 confocal microscope with a 63x HC PL APO CS2 glycerol objective NA 1.3. or a Zeiss LSM 880 using a 63x Plan Apochromat oil objective, NA 1.4. For all confocal microscopy experiments laser power, zoom factor, pixel size, bit depth and pinhole size was kept identical between treatments and imaging of different channels was performed sequentially. Pinhole size was kept at 1.0 Airy Unit (AU) for all experiments, except for experiments where endogenous ACSL3 or DGAT2 staining was examined, where pinhole of 0.6 Airy Unit was used to achieve enhanced resolution. This imaging regime was also used for representative images. For assessment of LD morphology, z-stacks were acquired with identical settings between time points and cell lines. For assessment of overexpressed transfected protein localization in cells, detector gain settings were adjusted to account for differences in expression levels. For imaging of EGFP, LD540 and mCherry signals, excitation was performed sequentially at wavelengths 478, 514 and 596 nm, respectively, and emission measured at 480-500 nm, 540-560 nm and 630-660 nm. Singly labeled specimens were used as controls to ensure that no cross-talk was recorded.

3D-SIM. Three-dimensional structured illumination microscopy was performed on a Deltavision OMX V4 microscope (Applied Precision, GE Healthcare) equipped with an Olympus 60x Plan Apochromat objective (NA 1.42), 488 nm and 568 nm laserlines, and three cooled sCMOS cameras. Z-stacks of the cell were recorded, with a z-spacing of 125 nm. For each focal plane, 15 raw images (5 phases for 3 different angular orientations of the illumination pattern) were captured. Images were reconstructed, aligned, and processed for presentation using Softworx software (Applied Precision, GE Healthcare), with a final voxel size of 40x40x125nm. WT-seipin-GFP association with LDs was manually analyzed in ImageJ FIJI. A puncta was considered LD-associated if, after background removal, there were no overlapping pixels between it and the LD. LD diameter was measured in ImageJ FIJI by drawing straight lines through the LD diameter and using an open access code to fit the intensity line profiles to a Gaussian curve and calculate the full width half maximum (FWHM) from the fitted curve (John Lim, March 2011).

STORM. Cells were grown on Mattek 35 mm petri dishes with thickness 1.5 cover glass, fixed and stained with anti-GFP and Alexa-647 antibodies. Widefield near-TIRF and STORM imaging was performed with Nikon Eclipse Ti-E N-STORM equipped with Apo TIRF 100x Vil objective (NA 1.49) and 300mW 647nm laser, using iXon+ 897 camera (Andor Technology). After antibody labeling, dishes were placed in STORM buffer (0.1 M Tris, pH 7.9, 10% glucose, 0.07 cysteamine, 0.75 mg/ml glucose oxidase, 0.04 mg/ml catalase) and then continuously illuminated at 647 nm (full power) and a series of 20 000 images (256x256 pixels, 16 ms exposure time) were acquired. The N-STORM software (Nikon) was used for the localization of single fluorophore activations and images were exported for analysis in ImageJ FIJI with 10 nm Gaussian rendering. The size of the resulting structures was estimated as described for LD diameter, by drawing two perpendicular lines through each structure, crossing at the estimated center of the structure of interest, and measuring the FWHM of those lines.

Live cell imaging. For live cell experiments cells were seeded onto 1 µ-slide 8 well ibiTreat chambers (ibidi, confocal and widefield live cell microscopy) or 8-well Lab-Tek II #1.5 coverglass slides (Lab-TEK, Airyscan live cell microscopy and FRAP experiments) coated with 10 µg/ml human fibronectin (Roche Diagnostics). All live cell imaging experiments were performed at +37°C, 5% CO_2 in indicated growth medium supplemented with OA as described. Imaging of end-seipin-sfGFP was done in FluoroBrite DMEM supplemented with Prolong Antifade (1:100).

LD size and LD motility analysis. Cells were imaged using Nikon Eclipse Ti-E N-STORM equipped with 60x PlanApo VC oil objective (NA 1.40) and 1.5 zoom lens and Andor iXon+ 885 EMCCD camera. For LD size analysis cells were fixed, stained with LD540 and DAPI and z-stacks were acquired and deconvolved. LD size measurements from ROIs (whole cells for 1 h OA, 15x15 µm peripheral areas with no LD clusters for 20 h OA) were performed with ICY software (de Chaumont *et al*, 2012) using Spot detector plugin with algorithms described in (Olivo-Marin, 2002). For LD mobility analysis image acquisition frame rate was 400 ms and LD mobility from resulting live cell videos was assessed by measuring the Pearson colocalization coefficient between subsequent frames/cell (A431 cells) or frames/ROI (20x20µm peripheral ROI, two ROIs/cell, fibroblasts), and decreased degree of colocalization was considered indicative of increased LD mobility. 10 initial frames from time-lapse acquisitions were included in the analysis for each cell. LD velocities of small peripheral LDs were further analyzed by manual tracking plugin in ImageJ FIJI (20-150 frames/track) and their size was measured in FIJI.

Airyscan live cell microscopy and analysis. Cells were imaged with a Zeiss LSM 880 equipped with an Airyscan detector using a 63x Plan Apochromat oil objective, NA 1.4. Airyscan technology provides an increase in the x-, y- and z- resolution with increased signal-to-noise-ratio (Weisshart, 2014). Live cell imaging was done in super resolution ILEX-mode, 16 bit depth, zoom factor 15 or 20 with constant pixel size of 44x44 nm, with sequential excitation of fluorophores using appropriate

lasers and stable emission filter sets. With this imaging regime crosstalk was minimal compared to signal, and singly labeled specimens were used as controls. The Airyscan detector was adjusted regularly between time-lapse acquisitions. For WT-seipin-GFP movement in relation to LDs, LDs were labeled with LipidTox Deep Red and acquisition rate was 375 ms (SKO + WT-Seipin-GFP) or 3 s (end-seipin-sfGFP). Seipin punctae movement as well as LD mobility from Airyscan videos was analyzed by manual tracking plugin in ImageJ FIJI (10-100 frames/track). For analysis of ER associated movement of nascent LDs, cells were transfected with sfGFP-ER-3 or BFP-KDEL, delipidated overnight and incubated with OA for 20-75 min. For analysis of ER associated movement of LDs present after longer fatty acid incubation, cells were transfected with ER marker plasmids as above and incubated with OA for 20 h. Imaging was done in the presence of OA and LD marker (Lipidtox Deep Red or LD540) with a frame rate of 165-195 ms (sfGFP-ER-3 and LipidTox Deep Red) or 195 ms (BFP-KDEL and LD540). Phenotyping and velocity measurements of LD ER-associated movement was done by manual tracking in ImageJ FIJI, only LDs visible during the first 20 frames of videos were included in the analysis. LDs were considered to belong to category i) if they only moved within a very short (circa <1µm) distance along the ER and/or if they moved together with the ER structure. LDs were considered to belong to category ii) if they showed clear mobility along ER structures, with ER junctions providing landmarks. LDs were considered to belong to category iii) if they showed a) at least one frame of over 140 nm apparent distance to nearest ER structure and b) movement did not occur along/with ER structures.

FRAP and Airyscan photobleaching experiments. Photobleaching experiments were conducted with Zeiss LSM 880. For HPos-Cherry and BPY-C12 photobleaching experiments the LDs were stained with LipidTox Green. A single LD was selected as ROI, bleached with iterations of 514 and 560 laser at full power, and recovery was monitored in ILEX mode (Airyscan experiments) or sequential confocal scanning (other experiments, with a pinhole of 2 AU). For Airyscan experiments, pixel size was 41x41 nm and frame rate 300 ms (BPY) or 1.5 s (HPos), and bleached ROI was 10

µm^2. For conventional FRAP experiments of HPos, pixel size was 60x60nm, frame rate 1s, bleached ROI was 1.9µm^2. For conventional FRAP experiments of BPY, pixel size was 90x90nm, frame rate 123 ms, bleached ROI was 1.6 µm^2. Images were analyzed in ImageJ FIJI, and the intensity of HPos or BPY-C12 in the ROI (LD) was analysed at each time point. Only LDs without significant z-drift (as visualised by the LD marker channel) were analyzed. Intensity was corrected for bleaching of the whole imaged cell area excluding bleached ROI, and normalized to pre-bleach intensity. Shown are double normalized curves, where post-bleach intensity was set to zero. For analysis, the individual measurements were averaged and the resulting kinetics were fitted with the 2-exponential model using a custom-made fitting function in Matlab (The MathWorks, Inc., Natick, MA).

Image processing. Airyscan videos and images were Airyscan-processed using the Zeiss Zen software package with identical (default) settings for all acquisitions. Deconvolution, where indicated, was performed in Huygens software (Scientific Volume Imaging) using iterative Classic Maximum Likelihood Estimation. For representative images brightness, contrast and scale bars were adjusted in ImageJ FIJI and Corel Draw X7.

Colocalization analysis. All colocalization analysis was performed in ImageJ FIJI. Analysis of fluorescent proteins and LD dyes was done with colocalization threshold plugin, employing auto-thresholding (Costes *et al*, 2004), performed after background subtraction. Shown are Mander's (m1) colocalization coefficients. Colocalization analysis of BPY-C12 LDs was performed with coloc 2 plugin after background subtraction. Analysis of endogenous ACSL3, HPos and seipin-GFP variants association with LDs was done by manual grouping in ImageJ FIJI using deconvolved or Airyscan-processed z-stacks.

Pre-embedding immuno-EM and quantification. For immunolocalization of proteins, cells were prepared for immunolabeling as described in (Salonen *et al*, 2003). Briefly, cells were fixed with

PLP-fixative (McLean and Nakane, 1974) for 2 h, permeabilized with 0.01% saponin for 8 min, labeled with anti-GFP (1 h) or anti-ACSL3 (2 h), incubated with nano-gold-conjugated anti-mouse FAB-fragments for 1 h (Nanoprobes, 1:60), post-fixed with 1% glutaraldehyde, and quenched with 50 mM glycine. Nano-gold particles were then intensified using the HQ SILVER Enhancement kit (Nanoprobes, Cat.No 2012) followed by gold toning in subsequent incubations in 2% NaAcetate, 0.05% $HAuCl_4$ and 0.3% $Na_2S_2O_3 \bullet 5H_2O$. The cells were processed for EM as described (Seemann *et al*, 2000). Ultrathin sections, cut using Leica UCT6 microtome, were picked on Pioloform coated single slot grids, post-stained with uranyl acetate and lead citrate, and observed with a Jeol JEM-1400 microscope (Jeol Ltd., Tokyo, Japan) operated at 80 kV. Images were acquired with Gatan Orius SC 1000B camera.

The distribution of the anti-GFP-labeling and of the organelles was quantified essentially as described in (Mayhew, 2011) using Microscopy Image Browser (MIB) software (Belevich *et al*, 2015). Briefly, to estimate the volumes of organelle compartments per image, a grid of 75 pixels between branch points was placed on each image and each branch point was assigned to one of the categories: 1) ER, 2) LD, 3) ER-LD contact, 4) other. Nuclei and extracellular area were excluded. Points per category were calculated. Clusters of immuno-gold were assigned to the same categories and calculated. Expected gold and relative labeling index was calculated as described (Mayhew, 2011). Assessment of ACSL3 labeling on LDs was done by imaging all LD profiles within one section of 8 randomly selected cells of each cell type and further analyzing the LDs with ER contact into categories based on ACSL3 labeling.

Serial block face scanning EM, image analysis and modeling. SB-EM samples were prepared as described in (Puhka *et al*, 2012) and images were acquired with a FEG-SEM Quanta 250 (FEI Company) equipped with a 3View-system (Gatan Inc.) for serial imaging of block faces using a backscattered electron detector (Gatan Inc.). The cells were imaged with 2.5 kV beam voltage, spot

size 3, and 0.3 Torr pressure, the voxel size was 20 x 20 x 40 nm. The images were processed and the models segmented using MIB (Belevich *et al*, 2015). The radii of LDs were measured using the Measure tool of MIB. The visualization of 3D models and measurements of the distances between LDs and ER profiles were performed in Amira (VSG, FEI Company).

Measurement of ER width from ultrathin TEM sections. Samples were prepared as in (Seemann *et al*, 2000). ER profile width was measured from TEM images taken at x8000 magnification using the Measure Tool of MIB (Belevich *et al*, 2015). For systematic random sampling, an evenly spaced 400 nm step grid was placed over the TEM images and the width of perpendicularly oriented ER profiles crossing the grid lines was measured.

Electron tomography and modeling. For 3D electron tomogprahy cells were grown on glass coverslips and fixed with 3% glutaraldehyde in 0.1 M Na-cacodylate buffer, pH 7.4, supplemented with 1 mM $CaCl_2$ and 0.1% malachite green. Malachite green was used to enhance preservation of lipids (Hayat, 1993). Specimens were osmicated with reduced osmium, stained with uranyl acetate *en bloc*, dehydrated and embedded in Epon resin (TAAB, Aldermaston, United Kingdom) as described in (Puhka *et al*, 2007). Dual axis tilt series (Mastronarde, 1997) were recorded from three consecutive semi-thick (250 nm) sections using Tecnai FEG 20 (FEI Corp.) microscope operating at 200 kV. The sections were tilted at 1-degree intervals using a high tilt specimen holder (model 2020; E.A. Fischione Instruments) between ±62 degrees. Images were acquired with SerialEM software (Mastronarde, 2005) using a 4k × 4k Ultrascan 4000 CCD camera (Gatan Corp.) at nominal magnification 7,800×, providing a 2×binned pixel size of 2.84 nm. The alignment of the tilt series as well as reconstructions were done with IMOD software package (Kremer *et al*, 1996) using 10-nm colloidal gold particles as fiducial markers. For manual segmentation and visualization, tomograms were denoised using nonlinear anisotrophic diffusion filter, K=1 for 4 iterations (Frangakis and

Hegerl, 2001). Tomographic reconstructions were segmented, modeled and visualized using MIB software (Belevich *et al*, 2015) and modeling, visualization and surface area measurements of LD and ER-LD contact profiles were performed in Amira (VSG, FEI Company).

Appendix references

Belevich I, Joensuu M, Kumar D, Vihinen H & Jokitalo E (2015) Microscopy Image Browser: A platform for segmentation and analysis of multidimensional datasets. *PLoS Biol.* **14(1)**:e1002340.

de Chaumont F, Dallongeville S, Chenouard N, Hervé N, Pop S, Provoost T, Meas-Yedid V, Pankajakshan P, Lecomte T, Le Montagner Y, Lagache T, Dufour A & Olivo-Marin J-C (2012) Icy: an open bioimage informatics platform for extended reproducible research. *Nat. Methods* **9:** 690–696

Costes S V, Daelemans D, Cho EH, Dobbin Z, Pavlakis G & Lockett S (2004) Automatic and quantitative measurement of protein-protein colocalization in live cells. *Biophys. J.* **86:** 3993–4003

Elbashir SM, Harborth J, Lendeckel W, Yalcin A, Weber K & Tuschl T (2001) Duplexes of 21 ± nucleotide RNAs mediate RNA interference in cultured mammalian cells. *Nature* **411:** 494–498

Frangakis AS & Hegerl R (2001) Noise reduction in electron tomographic reconstructions using nonlinear anisotropic diffusion. J. Struct. Biol. **135**:239–250.

Friedman JR, Lackner LL, West M, DiBenedetto JR, Nunnari J & Voeltz GK (2011) ER tubules mark sites of mitochondrial division. *Science* **334:** 358–362

Hayat MA (1993) Stains and Cytochemical Methods New York: Plenum Press

Hobbs S, Jitrapakdee S & Wallace JC (1998) Development of a bicistronic vector driven by the human polypeptide chain elongation factor 1alpha promoter for creation of stable mammalian cell lines that express very high levels of recombinant proteins. *Biochem. Biophys. Res. Commun.* **252:** 368–72

Hölttä-Vuori M, Salo VT, Ohsaki Y, Suster ML & Ikonen E (2013) Alleviation of seipinopathy-related ER stress by triglyceride storage. *Hum. Mol. Genet.* **22:** 1157–66

Kano F, Kondo H, Yamamoto A, Kaneko Y, Uchiyama K, Hosokawa N, Nagata K & Murata M (2005) NSF/SNAPs and p97/p47/VCIP135 are sequentially required for cell cycle-dependent reformation of the ER network. *Genes Cells* **10:** 989–99

Kassan A, Herms A, Fernández-Vidal A, Bosch M, Schieber NL, Reddy BJN, Fajardo A, Gelabert-Baldrich M, Tebar F, Enrich C, Gross SP, Parton RG & Pol A (2013) Acyl-CoA synthetase 3 promotes lipid droplet biogenesis in ER microdomains. *J. Cell Biol.* **203:** 985–1001

Kremer J, Mastronarde D & McIntosh J (1996) Computer visualization of three-dimensional image data using IMOD. *J. Struct. Biol.* **76:** 71–76

Kuerschner L, Moessinger C & Thiele C (2008) Imaging of lipid biosynthesis: how a neutral lipid enters lipid droplets. *Traffic* **9:** 338–52

Martell JD, Deerinck TJ, Sancak Y, Poulos TL, Mootha VK, Sosinsky GE, Ellisman MH & Ting AY (2012) Engineered ascorbate peroxidase as a genetically encoded reporter for electron microscopy. *Nat. Biotechnol.* **30:** 1143–8

Mastronarde DN (1997) Dual-axis tomography: an approach with alignment methods that preserve resolution. *J. Struct. Biol.* **120:** 343–352

Mastronarde DN (2005) Automated electron microscope tomography using robust prediction of specimen movements. *J. Struct. Biol.* **152:** 36–51

Mayhew TM (2011) Mapping the distributions and quantifying the labelling intensities of cell compartments by immunoelectron microscopy: progress towards a coherent set of methods. *J. Anat.* **219:** 647–60

McLean IW & Nakane PK (1974) Periodate-lysine-paraformaldehyde fixative. A new fixation for immunoelectron microscopy. *J. Histochem. Cytochem.* **22:** 1077–1083

Morgenstern JP & Land H (1990) Advanced mammalian gene transfer: high titre retroviral vectors with multiple drug selection markers and a complementary helper-free packaging cell line. *Nucleic Acids Res.* **18:** 3587–96

Olivo-Marin JC (2002) Extraction of spots in biological images using multiscale products. *Pattern Recognit.* **35:** 1989–1996

Puhka M, Joensuu M, Vihinen H, Belevich I & Jokitalo E (2012) Progressive sheet-to-tubule transformation is a general mechanism for endoplasmic reticulum partitioning in dividing mammalian cells. *Mol. Biol. Cell* **23:** 2424–32

Puhka M, Vihinen H, Joensuu M & Jokitalo E (2007) Endoplasmic reticulum remains continuous and undergoes sheet-to-tubule transformation during cell division in mammalian cells. *J. Cell Biol.* **179:** 895–909

Ran FA, Hsu PD, Wright J, Agarwala V, Scott D a & Zhang F (2013) Genome engineering using the CRISPR-Cas9 system. *Nat. Protoc.* **8:** 2281–308

Salonen A, Vasiljeva L, Merits A, Magden J, Jokitalo E & Kääriäinen L (2003) Properly folded nonstructural polyprotein directs the semliki forest virus replication complex to the endosomal compartment. *J. Virol.* **77:** 1691–702

Sander JD & Joung JK (2014) CRISPR-Cas systems for editing, regulating and targeting genomes. *Nat. Biotechnol.* **32:** 347–55

Seemann J, Jokitalo EJ & Warren G (2000) The role of the tethering proteins p115 and GM130 in transport through the Golgi apparatus in vivo. *Mol. Biol. Cell* **11:** 635–645

Spandl J, White DJ, Peychl J & Thiele C (2009) Live cell multicolor imaging of lipid droplets with a new dye, LD540. *Traffic* **10:** 1579–84

Thiele C, Papan C, Hoelper D, Kusserow K, Gaebler A, Schoene M, Piotrowitz K, Lohmann D, Spandl J, Stevanovic A, Shevchenko A & Kuerschner L (2012) Tracing Fatty Acid Metabolism by Click Chemistry.

Weisshart K (2014) The Basic Principle of Airyscanning. *Zeiss Microsc.*

Zhu X, Xu Y, Yu S, Lu L, Ding M, Cheng J, Song G, Gao X, Yao L, Fan D, Meng S, Zhang X, Hu S & Tian Y (2014) An efficient genotyping method for genome-modified animals and human

cells generated with CRISPR/Cas9 system. *Sci. Rep.* **4:** 6420

Appendix Figure legends

Appendix Figure S1. CRISPR targets and sequencing results of A431 WT and SKO cell lines used in this study.

Appendix Figure S2. In relation to Fig 1D. WT and SKO + WT-seipin-GFP cells were fixed and labeled as indicated and imaged with STORM. Dashed lines indicate cell boundaries.

Appendix Figure S3. In relation to Fig 1G, 1H. TEM micrographs visualizing larger fields of view verify the identification of ER profiles shown in Fig 1G and show the overall staining pattern. Boxed area is enlarged on the right.

Appendix Figure S4. (A) Schematic illustration of the generation of WT cells with seipin tagged at its chromosomal locus with superfolder (sf)-GFP using CRISPR/Cas9 technology. **(B)** Validation of the end-seipin-sfGFP cell line by Western blotting with anti-GFP and tubulin antibodies. 20 µg protein loaded/lane. Lane 1: WT A431 cells; lane 2: end-seipin-sf-GFP cells transfected with control siRNA for 3 days; lane3: end-seipin-sfGFP cells transfected with seipin siRNA for 3 days; lane 4: SKO cells stably expressing the short variant of seipin; lane 5: SKO cells stably expressing the long variant of seipin. Note that bands corresponding to both variants of seipin are detectable in end-seipin-sfGFP, and these bands are decreased by seipin siRNA treatment. Arrows indicate bands corresponding to the long and short form of GFP-tagged seipin.

Appendix Figure S5. (A) Airyscan video snapshots of end-seipin-sfGFP cells treated with OA for 20 h and imaged live in the presence of LipidTox Deep Red. Upper panels show a peripheral LD with end-seipin-sfGFP punctum associated (orange arrowhead). Note also more mobile non-LD associated

seipin puncta. Lower panels show an area of clustered LDs with end-seipin-sfGFP association. **(B)** In relation to Fig 6A. End-seipin-sfGFP cells were treated with OA for 1 h or 20 h, fixed and stained with LipidTox Red. Bars: % of LDs/cell with end-seipin-sfGFP association +/- SEM, n=4-7 cells. **(C)** SKO + WT or A212P-seipin-GFP cells were incubated with OA for 20 h, fixed and stained with anti-GFP antibodies and LD540 and imaged with Airyscan microscopy. Low-expressing cells were chosen for analysis to increase specificity, higher expressing cells can be seen in the periphery of the images. Maximum intensity projections of Airyscan z-stacks. Bars: % of LDs/ROI showing no seipin-GFP association, +/- SEM, n= 5 ROIs from 5 cells/genotype, 2 experiments, **p<0.005 (unpaired T-test). **(D)** WT and SKO cells were treated as in Fig 1A (1 h OA) or as in Fig 6B (20 h OA), fixed, and stained with LD540 and DAPI and imaged with widefield microscopy. Analysis from deconvolved z-stacks. Bars: total LD area/cell area, +/- SEM, n= 77-88 cells, 2 experiments, **p<0.005 (unpaired T-test). **(E)** WT and SKO cells were treated with OA for 20 h, LDs were labeled with LD540 and cells imaged live with widefield microsocpy. Shown are two subsequent frames (400 ms apart) and their overlap. Note the relative immobility of LD clusters (WT upper inset) and a large LD in SKO (SKO upper inset) compared to the highly mobile small peripheral LDs of SKO cells. **(F)** WT and SKO cells were transfected with ER-marker (sfGFP-ER-3) and incubated with OA for 20 h. LipidTox Deep Red was added prior to imaging to label LDs and cells were imaged live with Airyscan microscopy. Note the relative immobility and ER-association of WT clusters and large LDs in SKO cells. Orange arrowheads indicate peripheral, smaller LDs, moving along the ER (panel 2), or independent of the ER (panel 4). Note the different time scales. Signal intensities of images of later time points in panels 1 and 3 have been adjusted for bleaching. **(G)** Analysis of LD ER-associated movement of cells incubated with OA for 20 h. Analysis is performed as described in Fig 2F. Bars: % of LDs/ROI displaying indicated mode of movement, ± SEM, n= 35-41 ROIs (183-305 LDs), 2 experiments. **p<0.005 (Mann Whitney test). **(H)** WT and SKO cells were treated with OA for 20 h, processed for SB-EM and analyzed. Bars: number of LDs with no ER contacts/ROI, +/- SEM, n=

8 ROIs for WT (total volume analyzed 1274 μm^3), 6 ROIs for SKO (total volume analyzed 981 μm^3), 123-816 LDs. **(I)** WT and SKO cells were transfected with p-wt-human-DGAT2 and incubated with OA for 20 h, fixed and stained with anti-DGAT2 antibodies and LD540. Note the association of DGAT2 to many of the larger LDs in both WT and SKO cells.

Appendix Figure S6. WT and SKO cells stably expressing HPos-Cherry were incubated with OA for 20h, and LipidTox Green was added prior to imaging to label LDs. The HPos-Cherry signal on LDs was bleached and signal recovery to LDs monitored. This is an additional representation of the data in Fig 6J.

Appendix Figure S7. (A) Two control and BSCL2 fibroblast cell lines were treated with OA for 20 h, fixed and stained with LD540. Maximum intensity projections of deconvolved confocal z-stacks. **(B)** In relation to Fig 7D, 7E**.** Fibroblasts were transfected with ER marker plasmid (sfGFP-ER) for 24 h to label the ER and LD biogenesis was induced with OA incubation for 10-60 min. LipidTox Deep Red or LD540 was used to label LDs and cells were imaged live by Airyscan microscopy, Bars: mean velocity of tracked LDs in each group, ± SEM, n=37-82 LDs/group (130 LDs for control cells, 115 for BSCL2 cells), 2 experiments. *$p<0.05$, **$p<0.005$ (Kruskal-Wallis test, followed by Dunn test)**. (C)** In relation to Fig 7D, 7E. Analysis of maximum velocities (average between three subsequent frames) of tracked LDs in (B). Bars: mean maximum velocity of tracked LDs in each group, ± SEM, n=37-82 LDs/group (130 LDs for control cells, 115 for BSCL2 cells), 2 experiments, *$p<0.05$, **$p<0.005$ (Kruskal-Wallis test, followed by Dunn test). **(D)** Fibroblasts were transfected with ER marker (sf-GFP-ER-3) for 2 d and incubated with OA for 1 h, fixed and stained with LD540. Whole cell images are single confocal sections, insets represent maximum intensity projections of z-stacks of boxed regions. Four exemplary regions are shown. Orange arrowheads indicate LDs not in proximity to the ER. Representative of 3 acquisitions/genotype.

Appendix Figure S1.

Appendix Figure S2.

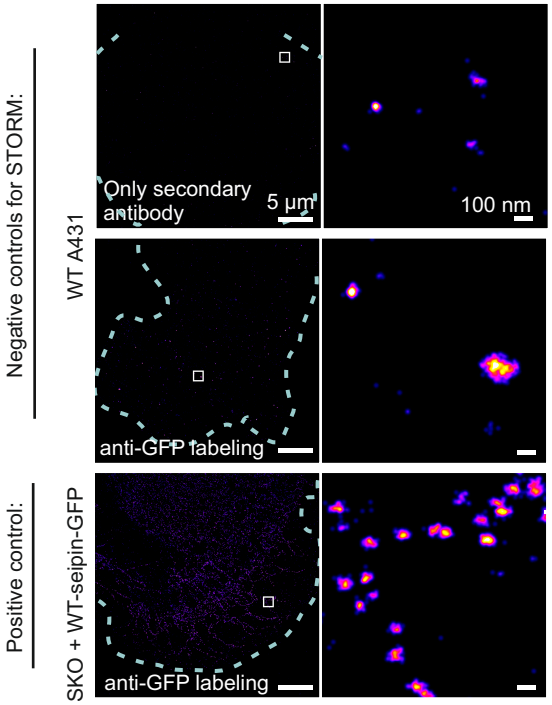

Appendix Figure S3.

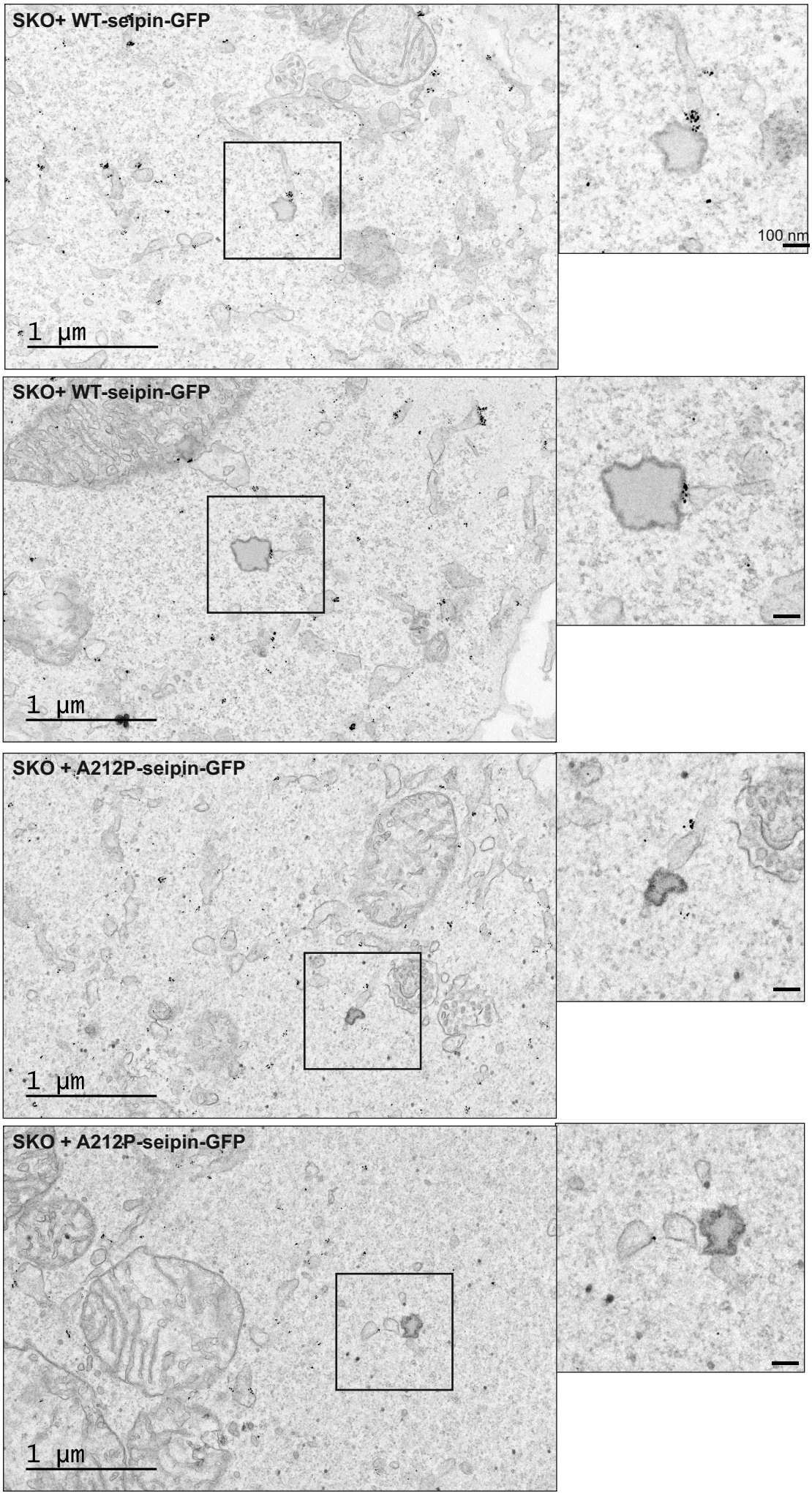

Appendix Figure S4.

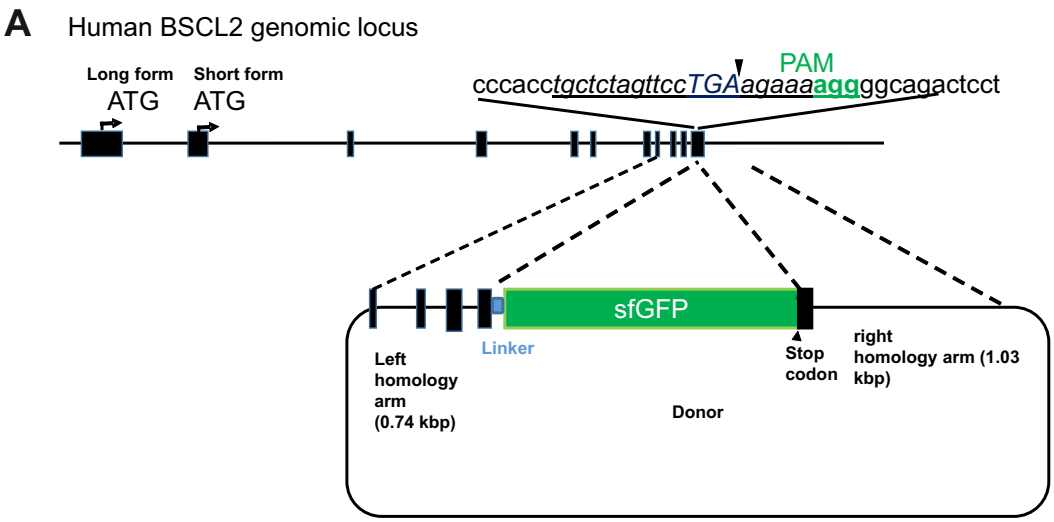

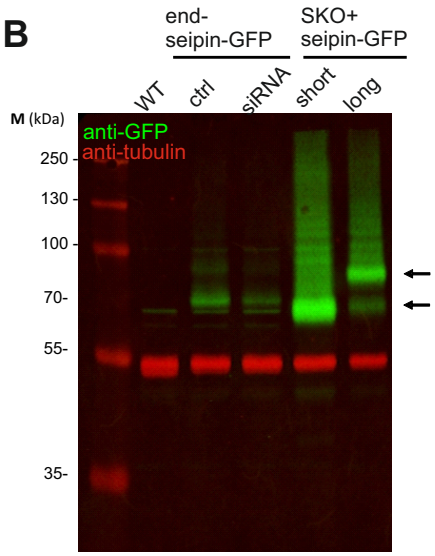

Appendix Figure S5.

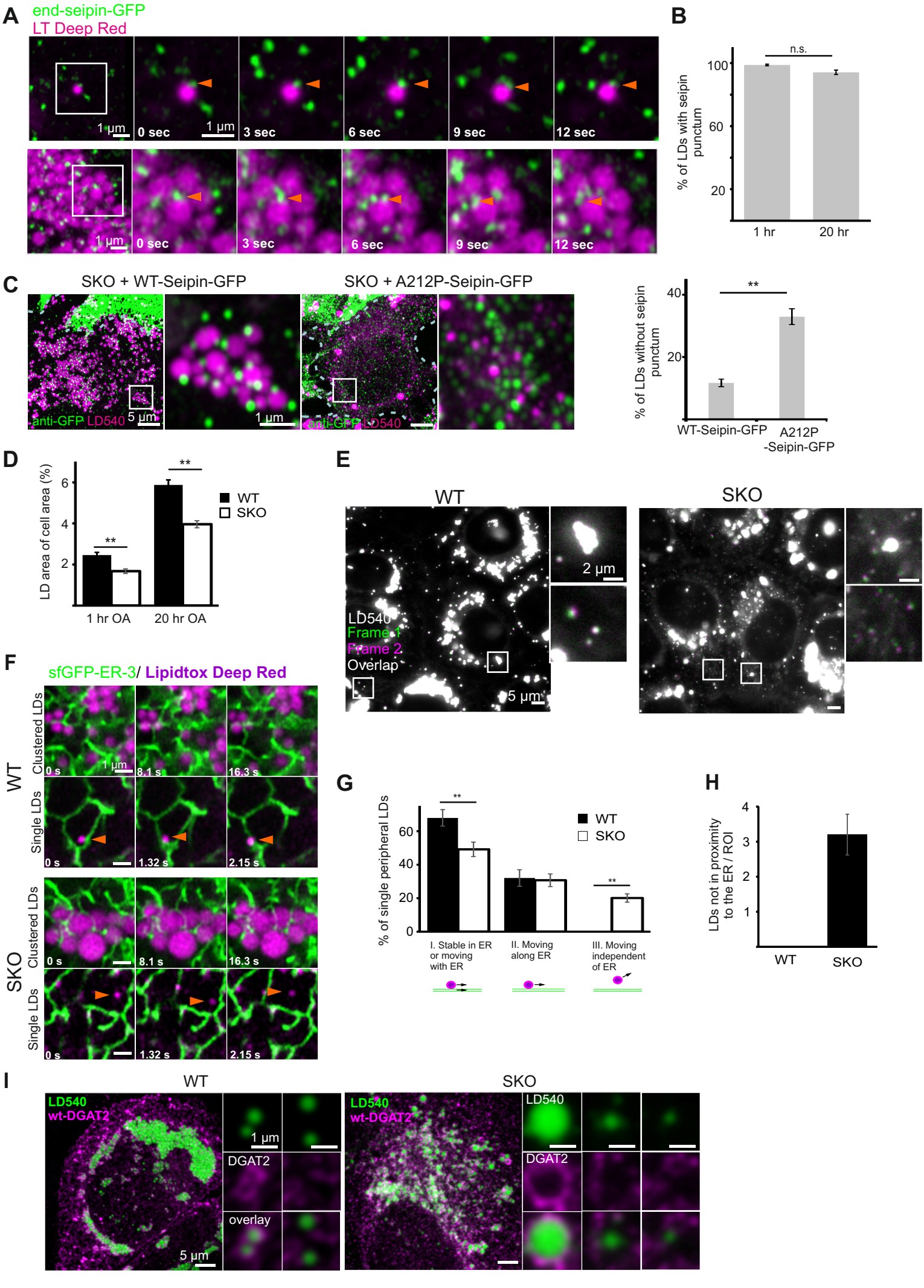

Appendix Figure S6.

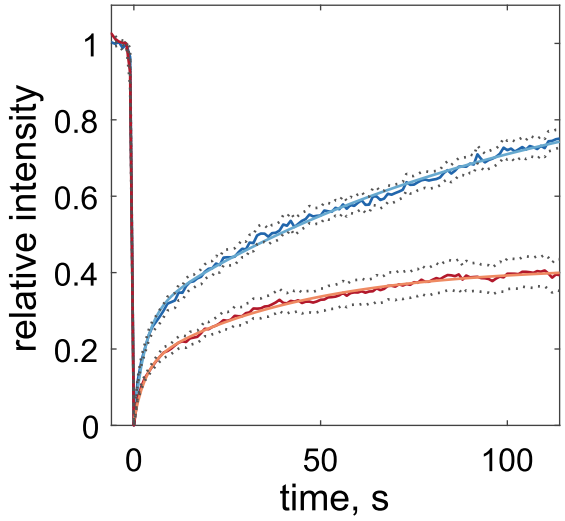

All WT LDs (n= 51)

$$f = -0.270 \cdot e^{-0.322t} - 0.678 \cdot e^{-0.010t} + 0.962$$

All SKO LDs (n= 61)

$$f = -0.141 \cdot e^{-0.331t} - 0.263 \cdot e^{-0.024t} + 0.417$$

Appendix Figure S7.

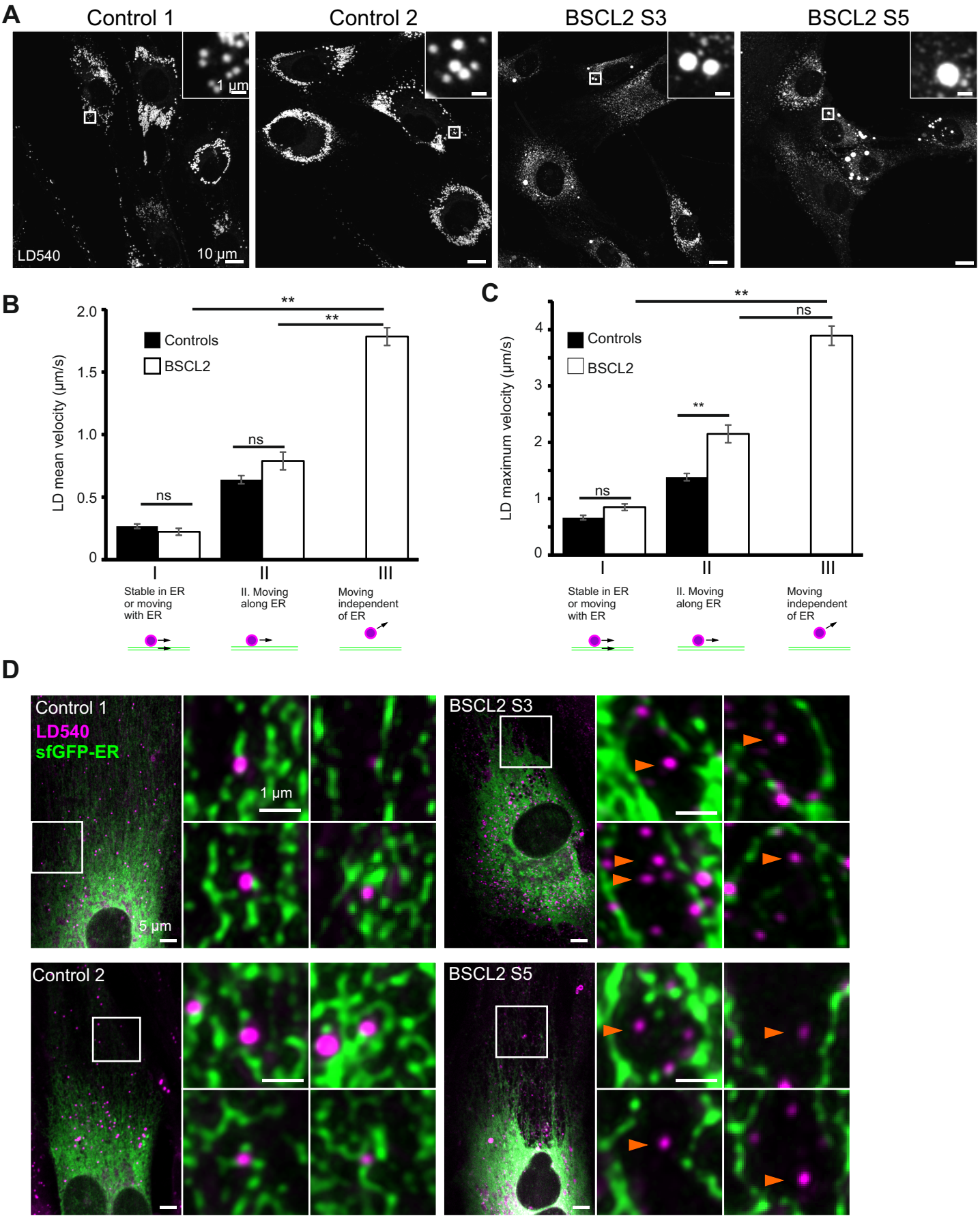

Appendix Table S1. Quantification of anti-GFP immunolabel in EM of SKO + WT-seipin-GFP cells

Compartment	Observed gold clusters	Gridpoints	Expected gold clusters	Relative labeling index (observed/expected)	χ^2
ER	2343	8392	358.9	6.5	10967.9
ER-LD contact	42	33	1.4	29.8	1167.3
LD	31	691	29.6	1.0	0.1
Other	1040	71690	3066.1	0.3	1338.9
Sum	3456	80806	3456		

Appendix Table S2. Quantification of anti-GFP immunolabel in EM of SKO+A212P-seipin-GFP cells

Compartment	Gold clusters	Gridpoints	Expected gold clusters	Relative labeling index (observed/expected)	χ^2
ER	2252	6934	287.2	7.8	13439.4
ER-LD contact	10	30	1.2	8.0	61.7
LD	23	482	20.0	1.2	0.4
Other	2227	101475	4203.6	0.5	929.4
Sum	4512	108921	4512		